Coherent Amplification and Noise in Gain-Enhanced Nanoplasmonic Metamaterials: A Maxwell-Bloch Langevin Approach

Andreas Pusch, Sebastian Wuestner, Joachim M. Hamm, Kosmas L. Tsakmakidis, and Ortwin Hess*

Blackett Laboratory, Department of Physics, Imperial College London, South Kensington Campus, London SW7 2AZ, United Kingdom

ABSTRACT

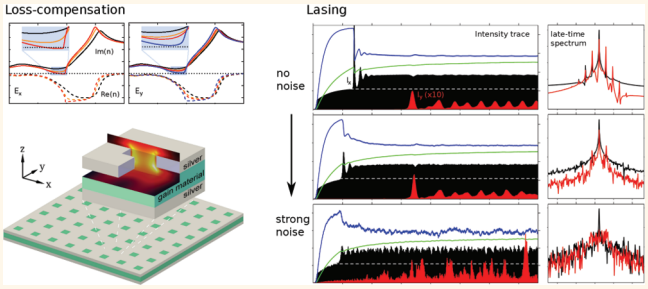

Nanoplasmonic metamaterials are an exciting new class of engineered media that promise a range of important applications, such as subwavelength focusing, cloaking, and slowing/stopping of light. At optical frequencies, using gain to overcome potentially not insignificant losses has recently emerged as a viable solution to ultra-low-loss operation that may lead to next-generation active metamaterials. Maxwell-Bloch models for active nanoplasmonic metamaterials are able to describe the coherent spatiotemporal and nonlinear gain—plasmon dynamics. Here, we extend the Maxwell-Bloch theory to a Maxwell-Bloch Langevin approach—a spatially resolved model that describes the light field and noise dynamics in gain-enhanced nanoplasmonic structures. Using the example of an optically pumped nanofishnet metamaterial with an embedded laser dye (four-level) medium exhibiting a negative refractive index, we demonstrate the transition from loss-compensation to amplification and to nanolasing. We observe ultrafast relaxation oscillations of the bright negative-index mode with frequencies just below the THz regime. The influence of noise on mode competition and the onset and magnitude of the relaxation oscillations is elucidated, and the dynamics and spectra of the emitted light indicate that coherent amplification and lasing are maintained even in the presence of noise and amplified spontaneous emission.

KEYWORDS: plasmonics · metamaterials · loss-compensation · amplification · nanolasing · Maxwell-Bloch theory · quantum noise

The conception and development of nanoplasmonic metamaterials has opened the door to the control of light fields on the nanoscale, a scale that is significantly smaller than the wavelength of visible light. Endowed with the possibility of such extreme control, metamaterials have been shown to enable the realization of materials with a vanishing or negative refractive index, inspiring applications in imaging (the "perfect lens"),[1,2] negative-index-based "invisibility" cloaking,[3] and even the stopping of light.[4,5] Unfortunately, in the optical regime, the absorption coefficients of passive negative-index metamaterials may be significant due to their nanoplasmonic constituents. Not surprisingly, intense efforts to conceive concepts that compensate the losses by enhancing metamaterials with gain media have recently been made.[6−15] Most prominently, it has been shown experimentally for the example of a double-fishnet metamaterial with incorporated laser dye[11] that the effective gain enhancement due to the nanoplasmonic environment enables the compensation of its internal dissipative losses. At the same time, it has become evident that engineering the emission properties of gain-enhanced plasmonic nanostructures and metamaterials in the loss-compensation regime and beyond (amplification, coherent emission, lasing, *etc.*) requires fundamental insight into the physical mechanisms underlying the nonlinear dynamical gain−plasmon interaction on the nanoscale. However, the conception of a comprehensive model encompassing all essential aspects of the physics of gain-enhanced nanoplasmonics and metamaterials has continued to present a substantial challenge. Indeed, such a description has to consider a number of physical and practical aspects, the integration of which into a single model is particularly demanding: First, nonlinearities, such as gain saturation, gain depletion, and spatial hole burning, may dominate the dynamics and thus the overall performance. Second, a plasmonic nanostructure/metamaterial is inherently structured on the nanometer scale, requiring a deep subwavelength spatial resolution and

* Address correspondence to o.hess@imperial.ac.uk.

Received for review December 2, 2011 and accepted February 13, 2012.

Published online February 13, 2012
10.1021/nn204692x

a full three-dimensional description to account for the relevant microscopic processes that affect the gain distribution, such as gain saturation and spatial inhomogeneities due to high field enhancements close to the metal. Third, quantum noise that leads to (amplified) spontaneous emission couples not only to the resonances of the meta-atoms but also to modes of the whole, often periodic, structure. In the light of recent advancements in quantum plasmonics[16,17] and with a view toward harnessing coherent amplification in nanoplasmonic metamaterials, an understanding of quantum noise in the coupling between plasmons and excitations is of fundamental importance. Finally, the modes of gain-enhanced nanoplasmonic metamaterials are quasi-modes that couple to the radiative continuum (photonic decay) and to electronic excitations in the metal (plasmonic decay). While approaches borrowed from quantum laser theory that build on discrete modes can make predictions about properties of conventional lasers, they are generally unable to deal with the quasi-modes in gain-enhanced nanoplasmonic metamaterials where there is spatiotemporal coherence in the gain material and spatiotemporal coherence in the plasmons that may in turn provide coherent feedback.

Here, we establish a Maxwell-Bloch Langevin approach linking stochastic four-level Langevin equations that grasp the quantum noise properties[18] of the gain medium and incorporate these into a previously developed semiclassical Maxwell-Bloch theory for gain-enhanced nanoplasmonic metamaterials.[12,19,20] This approach follows the spirit of time-domain models of noise as presented for a two-level gain medium[21] and successfully employed to describe properties of random lasers.[22] In our case of a gain-enhanced nanoplasmonic metamaterial, a unit cell of which is highlighted in Figure 1, optical pumping gives rise to a highly inhomogeneous inversion that dynamically affects the supported modes and their competition on the nanoscale. Therefore, a four-level model for the gain material is required. Note that, in the transmission/reflection direction, the system is, as expected from a system that is not opaque, modeled as an open system. Using the afore-described approach, we investigate the impact of (quantum) noise on the amplification process as evidenced in the relaxation oscillations in an optically pumped nanoplasmonic double-fishnet metamaterial. Owing to an inherently multimode nature and strong spatial hole burning effects, this gain-enhanced nanoplasmonic metamaterial brings together a rich variety of nonlinear phenomena, such as mode competition, ultrafast relaxation oscillation dynamics, and self-pulsations, the latter two with frequencies just below the THz regime.

The Maxwell-Bloch Langevin Approach. The Maxwell-Bloch Langevin (MBL) approach described here models the spatiotemporal interplay of coherent amplification and noise in gain-enhanced plasmonic nanostructures and metamaterials. Let us start by reminding us of the

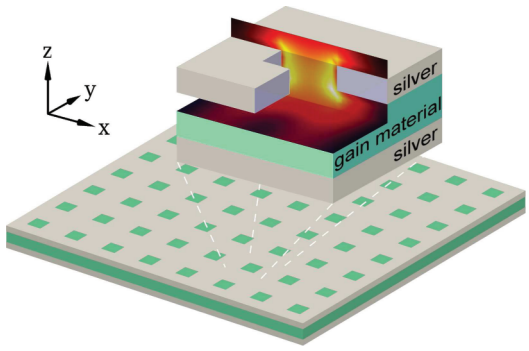

Figure 1. Gain-enhanced nanoplasmonic double-fishnet metamaterial. The gain material is embedded in the dielectric (turquoise) filling the space between the two perforated silver films (light gray) with parameters: period 280 nm, spacer height 70 nm, hole size 100 × 100 nm, metal thickness 40 nm, and refractive index of dielectric n_h = 1.62. The false color inset shows the plasmonic field enhancement at the pump wavelength in two planes within the unit cell. Brighter colors represent higher field enhancements.

essentials of the modeling of metals in nanoplasmonic materials. The spatiotemporal interaction of electromagnetic fields with the free electron plasma of a metal is the fundamental mechanism for the excitation and propagation of surface plasmons (SPs) on metal−dielectric interfaces. The Drude model is a simple but remarkably good response model that, when coupled to Maxwell's equations, accurately reproduces many features characteristic to these excitations. Here we are interested in the realistic modeling of SPs excited and localized on the thin nanostructured silver films embedded within the nanoplasmonic metamaterial structure. The model we adopt overlays a Drude response (D) with two Lorentzian resonances (L1,L2) to locally (at each point) create a response, which approximates experimentally measured thin-film data within a wavelength range λ = 300−800 nm. In this approach, the electric field $\mathbf{E}(\mathbf{x},t)$ dynamically drives three polarizations $\mathbf{P}_i(\mathbf{x},t)$, leading to

$$\begin{aligned}
\frac{\partial^2 \mathbf{P}_D}{\partial t^2} + \gamma_D \frac{\partial \mathbf{P}_D}{\partial t} &= \varepsilon_0 \omega_D^2 \mathbf{E} \\
\frac{\partial^2 \mathbf{P}_{L1}}{\partial t^2} + 2\gamma_{L1} \frac{\partial \mathbf{P}_{L1}}{\partial t} + \omega_{L1}^2 \mathbf{P}_{L1} &= \varepsilon_0 \Delta\varepsilon_{L1} \omega_{L1}^2 \mathbf{E} \qquad (1) \\
\frac{\partial^2 \mathbf{P}_{L2}}{\partial t^2} + 2\gamma_{L2} \frac{\partial \mathbf{P}_{L2}}{\partial t} + \omega_{L2}^2 \mathbf{P}_{L2} &= \varepsilon_0 \Delta\varepsilon_{L2} \omega_{L2}^2 \mathbf{E}
\end{aligned}$$

with parameters taken from McMahon *et al.*[23] We note that, in metamaterials, SP modes are excited when the propagating electromagnetic wave dynamically interacts with free electrons of the metallic nanostructure. Nonpropagating (localized) SP resonances, which can be excited inside a plasmonic resonator, are inherently lossy (ohmic losses) and couple to free-space photonic modes with a characteristic radiation damping rate. We emphasize that the resonant excitation, evolution, and temporal decay of both propagating and nonpropagating

(localized) SP modes emerge naturally from the presented model, and fundamental plasmonic spatiotemporal coherence is fully included.

Our approach combines the Drude-Lorentz material model for the metal with the Bloch equations for a four-level gain system as used for active nanoplasmonic metamaterials.[12,19,20] It enables us not only to describe on the nanoscale the spatiotemporal evolution of electromagnetic fields in arbitrary dielectric and nanoplasmonic geometries but also to include the spatiotemporal electronic responses of linear and nonlinear gain media. Here, we extend the model with Langevin terms to capture the noise induced by system−bath interactions in the gain medium. To allow for optical excitation, we model the optically pumped gain material as a four-level system with an optical transition for the absorption (0 ↔ 3) and for the emission (1 ↔ 2) as shown in Figure 2.

The two dipole transitions are phenomenologically coupled to form a four-level system by adding nonradiative carrier relaxation processes 3 → 2 and 1 → 0. Optical transitions between the subsystems (0,3) and (1,2) are considered to be dipole forbidden. We chose the parameters of the model to represent experimentally measured characteristics of Rhodamine 800.[24] The Lorentzian line shapes of the model provide an approximation to the actual line shapes as the measured line shapes of the absorption and emission lines arise from a combination of homogeneous broadening due to decoherence and inhomogeneous broadening due to a multitude of vibrational states. The polarization densities $\mathbf{P}_a = \mathbf{P}_a(\mathbf{x},t)$ of the transition 0 ↔ 3 and $\mathbf{P}_e = \mathbf{P}_e(\mathbf{x},t)$ of the transition 1 ↔ 2 are driven by the local electric field $\mathbf{E}(\mathbf{x},t)$ according to

$$\frac{\partial^2 \mathbf{P}_i}{\partial t^2} + 2\Gamma_i \frac{\partial \mathbf{P}_i}{\partial t} + \omega_{0,i}^2 \mathbf{P}_i = -\sigma_i \Delta N_i \mathbf{E}, \quad i = \mathrm{a,e} \qquad (2)$$

Here, $\Delta N_a(\mathbf{x},t) = N_3(\mathbf{x},t) - N_0(\mathbf{x},t)$ is the inversion of the absorption transition and $\Delta N_e(\mathbf{x},t) = N_2(\mathbf{x},t) - N_1(\mathbf{x},t)$ the inversion of the emission transition. We also introduce the resonance frequencies $\omega_{0,i} = (\omega_{r,i}^2 + \Gamma_i^2)^{1/2}$ and a phenomenological isotropic coupling constant σ_i. When the dye is optically pumped on the transition (0 ↔ 3), the four-level model will provide gain at the signal frequency *via* stimulated emission of the transition (1 ↔ 2). The inversion can then be harnessed as gain that is locally coupled into the electromagnetic fields with the local magnitude of the gain depending on the spatial distribution of the electric field and the inversion. Inherently included in the model are also the effects of gain saturation and depletion of the transitions which allows for the observation of nonlinearities such as pump saturation and gain depletion, manifesting themselves most strongly in pump/probe experiments.

The Maxwell-Bloch theory can be further extended to incorporate noise by adding stochastic Langevin

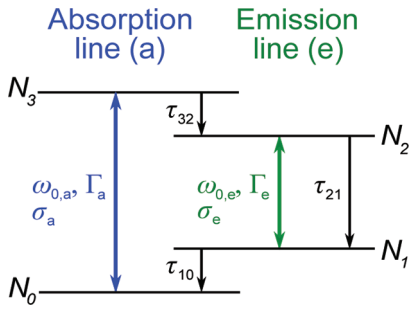

Figure 2. Sketch of the four-level system and its parameters.

terms. In the Methods section, we derive a second-order differential equation formalism—analogous to an existing Langevin approach for FDTD calculations of active two-level systems[21]—in which eq 12, eq 15, eq 17, and eq 18 combine to give the full set of equations for the four-level system

$$\begin{aligned}
\frac{\partial^2 \mathbf{P}_e}{\partial t^2} &= -2\Gamma_e \frac{\partial \mathbf{P}_e}{\partial t} - \omega_{0,e}^2 \mathbf{P}_e - \sigma_e (N_2 - N_1)\mathbf{E} \\
&\quad - \kappa_e \left(\omega_{0,e} \mathrm{Im}(\mathbf{F}_{12}) + \frac{\partial \mathrm{Re}(\mathbf{F}_{12})}{\partial t} \right) \\
\frac{\partial^2 \mathbf{P}_a}{\partial t^2} &= -2\Gamma_a \frac{\partial \mathbf{P}_a}{\partial t} - \omega_{0,a}^2 \mathbf{P}_a - \sigma_a (N_3 - N_0)\mathbf{E} \\
&\quad - \kappa_a \left(\omega_{0,a} \mathrm{Im}(\mathbf{F}_{03}) + \frac{\partial \mathrm{Re}(\mathbf{F}_{03})}{\partial t} \right)
\end{aligned} \qquad (3)$$

and

$$\begin{aligned}
\frac{\partial N_3}{\partial t} &= \frac{1}{\hbar \omega_{r,a}} \left(\frac{\partial \mathbf{P}_a}{\partial t} + \Gamma_a \mathbf{P}_a \right) \cdot \mathbf{E} - (\gamma_{32}^r + \gamma_{30}^r) N_3 + N_{\mathrm{cell}} F_{33} \\
\frac{\partial N_2}{\partial t} &= \frac{1}{\hbar \omega_{r,e}} \left(\frac{\partial \mathbf{P}_e}{\partial t} + \Gamma_e \mathbf{P}_e \right) \cdot \mathbf{E} + \gamma_{32}^r N_3 - \gamma_{21}^r N_2 + N_{\mathrm{cell}} F_{22} \\
\frac{\partial N_1}{\partial t} &= -\frac{1}{\hbar \omega_{r,e}} \left(\frac{\partial \mathbf{P}_e}{\partial t} + \Gamma_e \mathbf{P}_e \right) \cdot \mathbf{E} + \gamma_{21}^r N_2 - \gamma_{10}^r N_1 + N_{\mathrm{cell}} F_{11} \\
\frac{\partial N_0}{\partial t} &= -\frac{1}{\hbar \omega_{r,a}} \left(\frac{\partial \mathbf{P}_a}{\partial t} + \Gamma_a \mathbf{P}_a \right) \cdot \mathbf{E} + \gamma_{30}^r N_3 + \gamma_{10}^r N_1 + N_{\mathrm{cell}} F_{00}
\end{aligned} \qquad (4)$$

Here, $\kappa_{e,a}$ are the proportionality factors to transform $\mathrm{Re}(\rho_{12})$ to the polarizations $\mathbf{P}_{e,a}$ and $N_i = \rho_{ii} N_{\mathrm{cell}}$ the number of four-level systems in state i per unit volume (cell). The noise terms $F_{i,i}$, $i = 0...3$ for the occupation densities and F_{12} and F_{03} for the polarization terms are given in eq 17 and eq 18, respectively. Equations 3 and 4 together with eq 1, self-consistently coupled to the full time-domain 3D Maxwell equations, represent the basis of the Maxwell-Bloch Langevin approach to coherent amplification and noise in gain-enhanced plasmonic nanostructures and metamaterials.

RESULTS AND DISCUSSION

From Loss-Compensation to Coherent Amplification. Recently, it has been shown that dissipative (Ohmic) losses in negative-index metamaterials can be compensated in an ultrafast pump−probe setup where both the pump and the probe pulse were chosen to be shorter than the time scales on which typical fluctuations become relevant[12,19] and, crucially, where the gain provided was

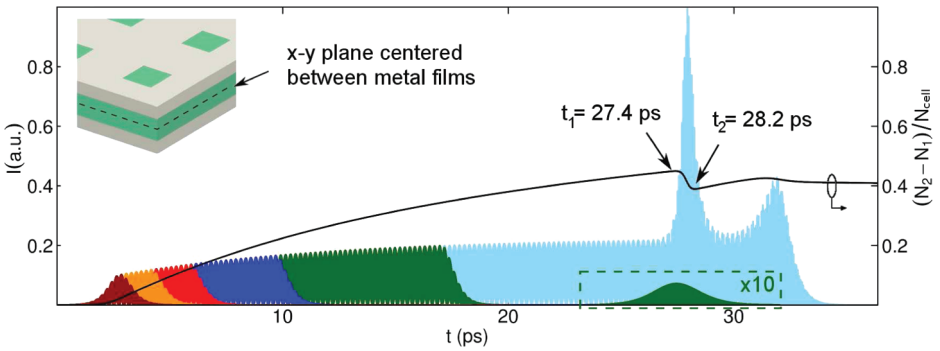

Figure 3. Transition from loss-compensation to coherent amplification to the onset of lasing. Far-field transmission of the optically pumped gain-enhanced double-fishnet metamaterial for varying duration τ_p of the optical pump intensity *I* (brown, 1.5 ps; yellow, 2.9 ps; red, 4.7 ps; blue, 8.5 ps; green, 15.8 ps; light blue, 30.5 ps) and average inversion $(N_2 - N_1)/N_{cell}$ of the gain material embedded in the fishnet (black line) for τ_p = 30.5 ps.

below the lasing threshold of the system. To directly link up with these studies, we will here initially suppress noise and explore the transition from ultrashort pulse to quasi-continuous wave (cw) optical pumping, and with increasing pump duration, we cross the lasing threshold of the bright negative-index mode. As a characteristic example of a gain-enhanced nanoplasmonic metamaterial, we will consider the symmetric nanoplasmonic double-fishnet structure, as depicted in Figure 1. We simulate the silver films (period 280 nm, spacer height 70 nm, hole size 100 × 100 nm, metal thickness 40 nm) on the basis of eq 1, and for the laser dye gain medium, modeled according to eq 3 and eq 4, we assume the following parameters: a density of $N = 2 \times 10^{19}$ cm^{-3}, emission and absorption wavelengths $\lambda_e = 2\pi c/\omega_{0,e} = 715$ nm and $\lambda_a = 690$ nm, coupling strengths $\sigma_e = 0.82 \times 10^{-8}$ C^2 kg^{-1}, $\sigma_a = 1.08 \times 10^{-8}$ C^2 kg^{-1}, dephasing rates $\Gamma_e = \Gamma_a = 40$ ps^{-1}, and relaxation rates $\tau_{30} = 0$, $\tau_{32} = \tau_{10} = 1/\gamma^r_{10} = 100$ fs and $\tau_{21} = 1/\gamma^r_{21} = 500$ ps.

In a sequence of numerical pump−probe experiments with a broad-band probe pulse, gradually increasing the duration of the optical pump, we progressively invert more and more of the laser dye gain medium inside the double-fishnet structure, reaching loss-compensation at the point when dissipative losses are overcome. Further increasing the pump duration (and thus the gain), we subsequently enter a regime of coherent amplification before radiative losses are overcome and lasing starts. Figure 3 shows the dynamic evolution of the transmitted field intensity with E_x-polarized pump pulses of increasing duration (from 1.5 ps to about 30 ps) and, for the case of the longest pulse with approximately 30 ps (light blue), the dynamics of the average inversion (black line) in the laser dye gain medium embedded within the double-fishnet structure. We can see that, as long as the system is pumped, the average inversion in the system gradually rises, providing more and more gain to probe light entering the system.

To extract effective electromagnetic parameters from the transmission, reflection, and absorption

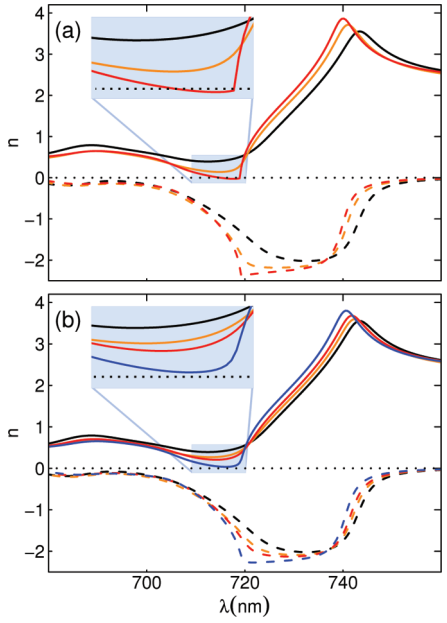

Figure 4. (a) Real (dashed lines) and imaginary parts (solid lines) of the refractive indices extracted for E_x-polarized probe light for the unpumped gain-enhanced fishnet metamaterial (black) and increasing pump durations from 1.5 ps up to 4.7 ps for E_x polarization and 8.5 ps for E_y polarization with color scheme as in Figure 3. (b) Same as (a) for *y*-polarized probe light.

spectra, we adopt the methodology of Smith *et al.*[25] (see the Methods section for details), and on its basis, we calculate the corresponding complex refractive index. Figure 4a shows the extracted dispersion of the real (dashed lines) and imaginary parts (solid lines) of the effective refractive indices for the structure when probed with E_x-polarized light; 2b portraits the corresponding case with E_y-polarized probe light. Increasing the pump duration before the probe pulse is launched leads, first, to a decrease in the absorption (characterized by Im(*n*)) and eventually to a negative Im(*n*), indicating that the structure has become amplifying instead of absorbing (red line in Figure 4a). A further increase in the pump duration results in the deposition of even more gain in the active nanostructure. In that regime, we find that the

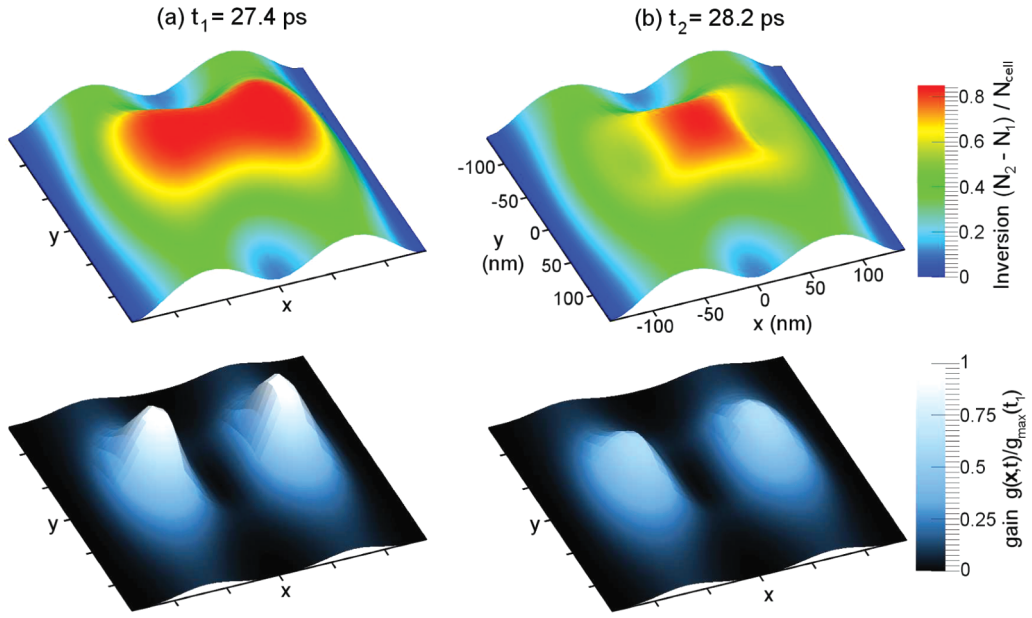

Figure 5. Snapshots of the spatial distribution of the inversion (top row) and the gain (bottom row) in the $x-y$ plane centered between the metal films at times just before and shortly after the lasing burst, as indicated in Figure 3.

effective parameters, as extracted by the standard retrieval method, exhibit discontinuities (data not shown here) despite the fact that the transmission/reflection/absorption spectra remain continuous (see also the Methods section).

An interesting point to note by comparing panels a and b of Figure 4a,b is that the effective refractive index of the gain-enhanced double-fishnet structure has become polarization-dependent despite the fact that the gain medium is isotropic. How is this possible? It is the different overlap of the gain inversion engendered by the E_x pump field with the modes for the two different polarizations that enables the E_x-polarized mode to exploit more gain than the E_y-polarized mode. Consequently, loss is not compensated in the E_y-polarized probe case, even for stronger pumping (see longer pulse duration, blue). This drastically demonstrates the important role of the spatiotemporal distribution of the inversion/gain in a gain-enhanced nanoplasmonic (metamaterial) structure.

This point is also evident when comparing the average inversion before and after the lasing burst which develops for a pumping level generated by the pump pulse with the longest duration (30.5 ps) that we have chosen in our study. Here, the spatially averaged inversion in the system has apparently only decreased marginally. Yet still the mode switches from being above threshold to below threshold. Indeed, while the average inversion only shows a surprisingly small decrease, at the points of high plasmonic field enhancement, however, the inversion $N_2 - N_1$ has decreased considerably (spatial hole burning), reducing the gain $g(\mathbf{x},t)$ delivered to the mode, given by the product of the mode's electric field profile and the inversion

$$g(\mathbf{x}, t) = \frac{\sigma E^2(\mathbf{x})[N_2(\mathbf{x}, t) - N_1(\mathbf{x}, t)]}{\int_V u(\mathbf{x})\mathrm{d}^3x} \quad (5)$$

Here, u is the energy density of the electromagnetic field. Figure 5a,b depicts the spatial inversion (top row) and gain distributions (bottom row) before (t_1 = 27.4 ps) and after (t_2 = 28.2 ps) the lasing burst, respectively; the times are indicated in Figure 3. One can clearly see the inhomogeneity of the gain and the significant depletion in the regions where the lasing mode, imprinted in the gain $g(\mathbf{x},t)$, exhibits high field enhancement. Indeed, the lasing burst burns a hole into the spatial inversion that strongly reduces the overall gain available to the mode because the inversion is reduced most strongly where the electric field is highest and where most of the gain was previously provided to the mode.

Figure 3 also shows that even for a shorter pulse duration (green) a small lasing burst is starting to arise long after the pump pulse has passed, albeit much less intense than the lasing burst for the longer pump duration. This indicates that apparently the gain-enhanced double-fishnet system has already reached threshold long before the lasing actually sets in. The slow onset of lasing can be attributed to the absence of noise in the numerical simulation. Here, it becomes most evident that while it is generally advantageous to include noise (and resulting amplified spontaneous emission) in a description of gain-enhanced plasmonic nanostructures/systems or metamaterials, it is imperative to do so if the system is coherently pumped above the lasing threshold. In the next section, we will

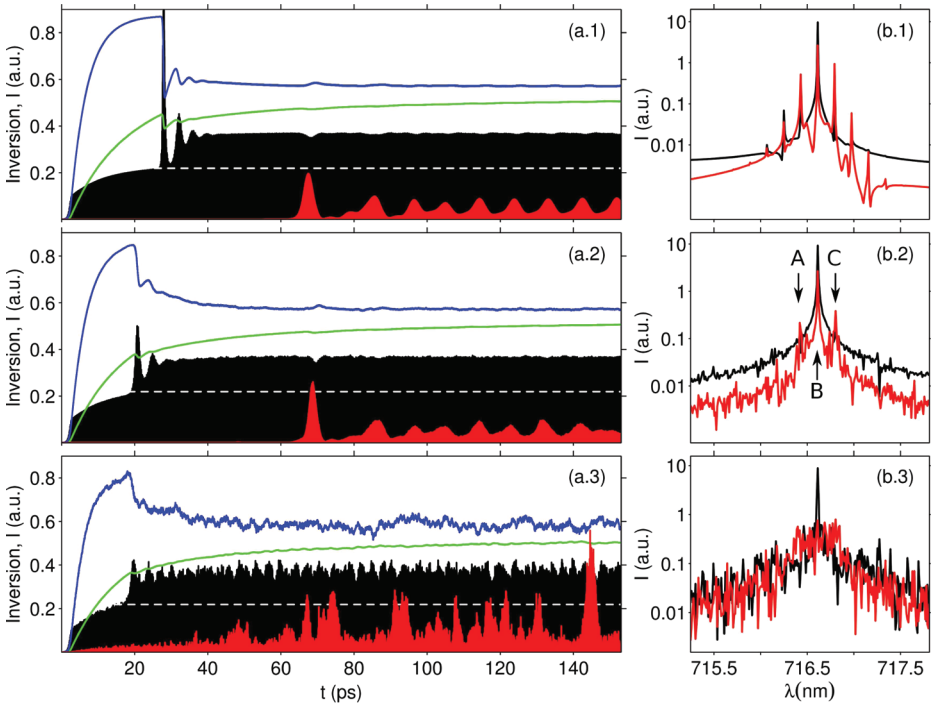

Figure 6. Ultrafast optical relaxation oscillations and nonlinear mode competition in a gain-enhanced nanoplasmonic fishnet metamaterial. (a) Dynamics of the inversion at a point of high field enhancement of the E_x-polarized mode (blue line), the average inversion across the unit cell (green line), and the intensity of E_x- (black line) and E_y-polarized emission (red line) for different noise levels. The intensity of E_y-polarized emission is scaled up by a factor of 20. (1) No noise, (2) moderate noise levels, and (3) strong noise. The white dashed line gives the approximate level of the pump intensity transmitted through the double-fishnet in steady state. (b) Intensity spectra taken from 50 ps onward for E_x- (black line) and E_y-polarized emission (red line). A, B, and C in b.2 indicate the wavelengths of the mode profiles shown in Figure 7.

therefore proceed to discuss the consequences of the inclusion of noise into our model using the Maxwell-Bloch Langevin approach introduced above.

Ultrafast Relaxation Oscillation Dynamics and Nonlinear Mode Competition. Having just seen that, for our system, coherent optical pump pulses shorter than about 10 ps result in loss-compensation and amplification but that for $\tau_p \gg 10$ ps lasing instabilities set in, we now specifically investigate the influence of noise on coherent amplification, again for our example of a three-dimensional gain-supplemented nanoplasmonic double-fishnet metamaterial (see Figure 1). The parameters used for gain material and E_x-polarized pump are kept, but now we investigate the regime of cw pump in the presence of three different noise levels: (1) no noise, (2) moderate noise, (3) strong noise (see Methods for a definition of the noise levels).

In order to observe relaxation oscillations—the signature and fingerprint of coherent amplification and lasing—both dissipative and radiative losses in the metamaterial film have to be overcome by the gain provided through inversion of the gain medium (four-level system).[20] Here we have designed the nanoplasmonic fishnet metamaterial such that the negative-index resonance band is in resonance with the emission wavelength of the gain medium. A good spatial overlap between inversion and the mode profile of this resonance is achieved by choosing a pump wavelength between the extraordinary transmission and negative-index resonances.[26] The double-fishnet structure investigated here is symmetric in the $x-y$ plane so that the E_x- and E_y-polarized resonances are degenerate. By coherent optical pumping with an E_x-polarized field, the symmetry of the system is broken as the inversion profile created by the pump overlaps more strongly with the E_x-polarized mode (see Figure 1 for the field enhancement of the pump). Therefore, it is expected that relaxation oscillations will first set in for the E_x-polarized negative-index mode but that the E_y-polarized mode may still reach threshold. As we will show below, the coexistence of both modes can lead to nonlinear mode competition.

Figure 6 shows the emission dynamics and emission spectra of the nanoplasmonic double-fishnet metamaterial. To demonstrate the influence of noise of variable magnitude on the THz emission dynamics and respective spectra, we show the case without noise (1) in comparison with moderate noise levels (2) and high levels of noise (3). In the absence of noise, the ultrafast relaxation oscillations in the E_x-polarized emission begin only after the build up of excess inversion above the steady-state value. The relaxation oscillations start with a high peak, are smooth, strongly damped, and have a frequency of approximately 250 GHz. The introduction of moderate noise shifts the onset of the relaxation oscillations to an earlier time, thereby

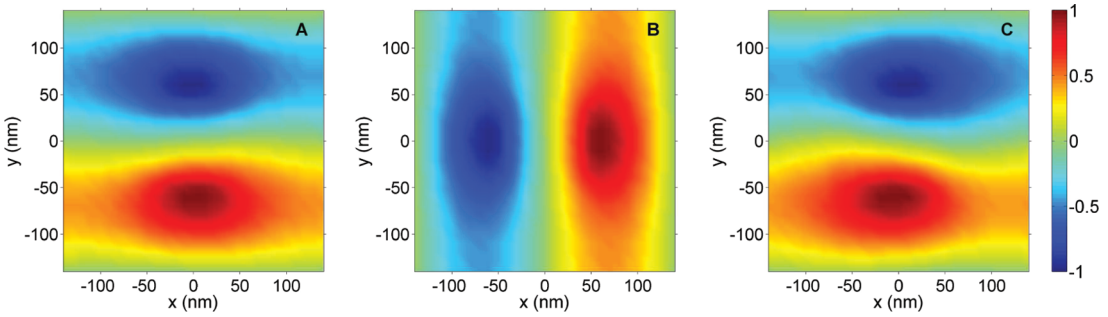

Figure 7. Mode profiles of the electric field E_z in the $x-y$ plane centered between the metal films of the double-fishnet at the wavelengths corresponding to the peaks in the intensity spectra of Figure 6b.2: A = 716.43 nm, B = 716.61 nm, and C = 717.79 nm. The field strengths are normalized to the maximum field amplitude at each wavelength.

reducing their amplitude while the smoothness of the curves is still retained to a good degree.

From Figure 6, we observe in both the field and inversion dynamics that the magnitude of the relaxation oscillation peaks is reduced when noise is present. In the strong noise case, relaxation oscillations are barely discernible but the system still lases, as can be seen from the spectrum in Figure 6b.3. The inclusion of noise impacts even more strongly on the E_y-polarized emission (red lines in Figure 6). By pumping the nanoplasmonic structure with E_x-polarized light, we have broken its inherent structural symmetry in the $x-y$ plane, and consequently, emission into the E_x-polarized mode is then favored. Nonetheless, even in the absence of noise, the E_y-polarized resonance eventually reaches threshold for coherent amplification in spite of lasing on the E_x-polarized mode. We note that the onset of the relaxation oscillation in the E_y-polarized mode can be seen as a small dip in the E_x-polarized emission. Contrary to the E_x-polarized mode, steady-state emission is not reached for the E_y-polarized mode; instead, self-pulsation is observed at a frequency of around 100 GHz. We attribute this self-pulsation to nonlinear mode competition between the E_x- and E_y-polarized modes through spatial hole burning.[27] The introduction of noise does not immediately lead to qualitative changes in the E_y-polarized emission. However, for strong noise, the E_y-polarized mode is characterized by a broader emission spectrum and never enters into a coherently emitting state, and internally, only amplified spontaneous emission is observed. Still the intensity spectra in Figure 6b.3 reveal that the emitted E_x-polarized field largely retains its frequency purity as is evident from the narrow line width of the emitted intensity.

At a position of high field enhancement of the E_x-polarized mode (chosen for the blue line in Figure 6), we observe a strong, phase-shifted imprint of the relaxation oscillations on the local inversion. In the absence of noise, the local inversion rises to a value of above 0.85 and the pumping saturates before lasing sets in with strong relaxation oscillations that deplete the gain. After rapidly damped oscillations, a steady-state local inversion is reached. For strong noise, however, the inversion jitters around the steady-state value even for late times. The jitter induced by noise is greatly reduced in magnitude when looking at the average inversion (green line). This indicates that the noise on the inversion is, to a large degree, independent across the unit cell. Interestingly, the average inversion continues to rise with the onset of lasing and reaches a steady-state value at a much later time. However, once relaxation oscillations set in, the average inversion is only reduced intermittently. The stark difference between the dynamics of the local inversion and the average inversion illustrates the importance of an approach with spatio-temporal resolution. Indeed, important parameters, such as lasing thresholds of modes, are determined by the intensity-weighted average over the inversion, which can be very different from the average inversion, in particular, due to the presence of (nonlinear) gain.

We noted above that the E_y-polarized mode can reach threshold long after lasing in the E_x-polarized mode has set in. This is because the inversion is still rising at points where the field enhancement of the E_x-polarized mode is low, reflected in the rise of the average inversion after the initial relaxation oscillations. Since the overlap between the two modes is not very strong (see Figure 7), regions of low field enhancement of the E_x-polarized mode can have a high field enhancement of the E_y-polarized mode. The inversion in regions where field enhancement is simultaneously low for the E_x-polarized mode and high for the E_y-polarized mode allows this spatially discriminated mode to come above threshold. When the E_y-polarized emission sets in, the inversion at the position of high field enhancement of the E_x resonance increases whereas the average inversion decreases. The first can be understood by observing that the E_x-polarized emission has, due to nonlinear mode competition, a dip at the onset of lasing into the second resonance thus for a short time allowing the inversion to rise at positions where the E_y-polarized resonance only has a weak electric field. This rise in inversion subsequently enhances the emission into the E_x-polarized resonance suppressing again the E_y-polarized resonance.

Self-pulsations, clearly seen in the much weaker E_y-polarized emission, are the consequence of this mode competition for the gain.

The intensity spectra presented in Figure 6b show that the emission is significantly shifted from the gain resonance at 715 to 716.61 nm. Considering that the "cold-cavity" resonance is also around 715 nm, this wavelength shift clearly indicates that the "nanoplasmonic hot-cavity" resonance is shifted from the cold-cavity resonance. The (later-time) far-field emission spectra show a narrow lasing peak in the E_x-polarized emission (black lines). Distinct side peaks with $\Delta\omega \approx 100$ GHz (the self-pulsation frequency) are apparent in the coherent spectrum and disappear when noise is introduced. Instead, noise significantly raises the background and leads to irregular peaks around the main emission. The differences between the spectra are more accentuated in the spatially discriminated E_y-polarized mode (red lines). In the strong noise case, the spectrum changes from a lasing spectrum to a broad amplified spontaneous emission spectrum. Amplified spontaneous emission can thus shift the lasing threshold sufficiently to suppress lasing into the E_y-polarized mode.

Figure 7 shows the mode distributions for the case of moderate noise at three different wavelengths (indicated in Figure 6b.2 by A, B, and C), corresponding to the central lasing peak and the first side-peaks in the spectrum. These results confirm that the central lasing peak of the E_x-polarized resonance dominates the electric field distribution showing a nodal line at $x = 0$. The field profiles of the side peaks display a nodal line at $y = 0$, indicating the predominance of E_y-polarized emission at these wavelengths. This observation agrees well with the spectrum for moderate noise in Figure 6b.2, where the side peaks of the E_y-polarized emission are substantially higher than the E_x-polarized emission at the same wavelength.

CONCLUSION

We have presented a spatiotemporal Maxwell-Bloch Langevin approach describing the interplay of coherent and incoherent light field and noise dynamics in gain-enhanced nanoplasmonics and metamaterials. With the example of a symmetric, optically pumped nanoplasmonic double-fishnet metamaterial with an embedded laser dye (four-level) medium exhibiting a negative refractive index, we have demonstrated the possibility of compensating characteristic Ohmic losses by gain. In spite of the inherent structural symmetry, a polarized pump field can induce a gain-related polarization anisotropy due to the distribution of the inversion. Following loss-compensation, it was shown that with increased pumping there first is a broad window of amplification before a lasing instability triggers coherent ultrafast relaxation oscillations of the bright negative-index mode with frequencies just below the THz regime. Under strong continuous pumping, the degenerate E_x- and E_y-polarized modes compete for gain and enter into a self-pulsating state. Studying the effect of noise strength on the spatiotemporal external and internal field dynamics, we have demonstrated that, although the details of the dynamics and spectral response depend on the noise magnitude, the emitted optical field can exhibit coherent amplification and lasing in the presence of strong noise.

METHODS

Noise in Two-Level Equations with Real-Valued Polarization. The Maxwell-Bloch equations for a two-level system under optical excitation may be considered as the minimal model for a dipolar optical transition in a discrete electronic system. An interaction with reservoirs is included *via* phenomenological dissipation terms, namely, the relaxation and dephasing rates. Because the dynamics of the reservoirs (baths) themselves are external to the core system describing the level dynamics, the damping of the system is accompanied by stochastic forces acting back onto the system.

Assuming Markovian noise correlations, the dynamics of an operator $\hat{A}$ that describes an observable of the reduced system can be approximated as[28]

$$\frac{\partial \hat{A}(t)}{\partial t} = \frac{1}{i\hbar}[\hat{A}(t), \hat{H}_s(t)] + \hat{D}(t) + \hat{F}(t) \tag{6}$$

where $\hat{H}_s$ represents the projection of the total Hamiltonian onto the reduced system and $\hat{D}$ and $\hat{F}$ are the effective dissipation and noise operators, respectively, arising from the interaction with the reservoir. The two-time correlation of the stochastic term $\hat{F}$ is determined by the fluctuation−dissipation theorem:

$$\langle \hat{F}(t)\hat{F}(t')\rangle = 2\langle \hat{D}(t)\rangle \delta(t - t') \tag{7}$$

The Markovian Langevin equations for the expectation values of the density matrix elements of a two-level system under optical excitation can then be formulated as[21,28,29]

$$\begin{aligned} \frac{\partial \rho_{12}}{\partial t} &= i(\rho_{12}\omega_r + \Omega_{12}(\rho_{11} - \rho_{22})) - \gamma_l \rho_{12} + \Gamma_{12} \\ \frac{\partial(\rho_{22} - \rho_{11})}{\partial t} &= 4\mathrm{Im}(\Omega_{12}\rho_{12}) - \gamma^r(\rho_{22} - \rho_{11} + 1) + \Gamma_{\mathrm{inv}} \end{aligned} \tag{8}$$

with

$$\begin{aligned} \Gamma_{12} &= (\xi_1 + i\xi_2)\sqrt{\frac{(\gamma_l - \gamma^r/2)(1 + \rho_{22} - \rho_{11})}{2N}} \\ \Gamma_{\mathrm{inv}} &= \xi_{\mathrm{inv}}\sqrt{\frac{2\gamma^r(1 + \rho_{22} - \rho_{11})}{N}} \end{aligned} \tag{9}$$

and $\Omega_{12} = |\mu_{12}\cdot \mathbf{E}|/\hbar$ is a classical, coherent electric field driving the atomic two-level system *via* its dipole moment μ_{12}. We ignore thermal fluctuations which are negligibly small at optical frequencies. The ξ_i are real, Gaussian, random variables fulfilling the two-time correlation

$$\langle \xi_i(t)\xi_{i'}(t')\rangle = \delta_{ii'}\delta(t - t') \tag{10}$$

N is the number of atoms in the volume represented by the grid cell. For a 3D simulation of a complete system, this is simply the number of atoms per dx^3. In 1D or 2D simulations, the grid cell

can represent a much larger volume; in the 1D case, it is $A dx$, where A is the cross-sectional area of the neglected dimensions; in the 2D case, it is $L dx^2$, where L is the extension of the system in the third dimension. We express this ratio between the number of atoms in a grid cell and the number of atoms in the physical volume represented by the grid cell by a factor ζ, so that $N = N_{\text{cell}}\zeta$.

In the second-order in time real polarization approach taken for the four-level system, the polarization **P** is proportional to the real part of the expectation value of the density matrix element $\langle\hat{\rho}_{12}\rangle = \rho_{12}$, whereas the imaginary part of the expectation value is given by[19]

$$\mathrm{Im}(\rho_{12}) = \frac{1}{\omega_r}\left(\frac{\partial \mathrm{Re}(\rho_{12})}{\partial t} + \gamma_l \mathrm{Re}(\rho_{12})\right) \tag{11}$$

Although the polarization is now reduced to a single real number, the noise associated with it is still expressed by two independent random numbers. The second-order in time equation containing Langevin terms for the real part of ρ_{12} can then be expressed as

$$\begin{aligned}\frac{\partial^2 \mathrm{Re}(\rho_{12})}{\partial t^2} = & -2\gamma_l \frac{\partial \mathrm{Re}(\rho_{12})}{\partial t} - (\omega^2 + \gamma_l^2)\mathrm{Re}(\rho_{12}) \\ & - \omega_r \frac{\mu \cdot \mathbf{E}}{\hbar}(\rho_{22} - \rho_{11}) - \omega_r \mathrm{Im}(\Gamma_{12}) + \frac{\partial \mathrm{Re}(\Gamma_{12})}{\partial t}\end{aligned} \tag{12}$$

and the equation for the occupation density is given by

$$\frac{\partial \rho_{22}}{\partial t} = 2\frac{\mu \cdot \mathbf{E}}{\hbar\omega_r}\left(\frac{\partial \mathrm{Re}(\rho_{12})}{\partial t} + \gamma_l \mathrm{Re}(\rho_{12})\right) - \gamma^r \rho_{22} + \frac{\Gamma_{\text{inv}}}{2} \tag{13}$$

Four-Level Langevin Equations. The four-level system consists of two individual two-level systems (3 ↔ 0 and 2 ↔ 1) which are connected *via* nonradiative recombination from levels 3 to 2 (γ^r_{32}) and 1 to 0 (γ^r_{10}). These two additional nonradiative, dissipative processes require additional Langevin noise terms. Furthermore, the noise terms of the previously discussed case of a two-level system have been derived under the assumption of $\rho_{22} + \rho_{11} = 1$, whereas now $\rho_{33} + \rho_{22} + \rho_{11} + \rho_{00} = 1$. We also note that now the additional decay channels modify the noise on the polarization and occupation densities. It is therefore necessary to rederive the noise terms starting from the fluctuation−dissipation theorem[18]

$$\langle \hat{F}_l(t)\hat{F}_m(t)\rangle = 2\langle \hat{D}_{lm}(t)\rangle$$

$$2\langle \hat{D}_{lm}\rangle = \left(\frac{d}{dt}\langle \hat{A}_l \hat{A}_m\rangle\right)_{\text{NH}} - \langle \hat{D}_l \hat{A}_m\rangle - \langle \hat{A}_l \hat{D}_m\rangle \tag{14}$$

where the time derivative includes only the non-Hamiltonian (dissipative) terms, $\hat{D}_l$ are the dissipation terms associated with the operators $\hat{A}$, and the mean values correspond to entries of the density matrix.

The equations for the density matrix of the four-level system are

$$\begin{aligned}\frac{\partial \hat{\rho}_{12}}{\partial t} &= i(\hat{\rho}_{12}\omega + \Omega_{12}(\hat{\rho}_{11} - \hat{\rho}_{22})) - \Gamma_e \hat{\rho}_{12} + \hat{F}_{12} \\ \frac{\partial \hat{\rho}_{03}}{\partial t} &= i(\hat{\rho}_{03}\omega + \Omega_{03}(\hat{\rho}_{00} - \hat{\rho}_{33})) - \Gamma_a \hat{\rho}_{03} + \hat{F}_{03} \\ \frac{\partial \hat{\rho}_{00}}{\partial t} &= -2\mathrm{Im}(\Omega_{03}\hat{\rho}_{03}) + \gamma^r_{10}\hat{\rho}_{11} + \gamma^r_{30}\hat{\rho}_{33} + \hat{F}_{00} \\ \frac{\partial \hat{\rho}_{11}}{\partial t} &= -2\mathrm{Im}(\Omega_{12}\hat{\rho}_{12}) + \gamma^r_{21}\hat{\rho}_{22} - \gamma^r_{10}\hat{\rho}_{11} + \hat{F}_{11} \\ \frac{\partial \hat{\rho}_{22}}{\partial t} &= 2\mathrm{Im}(\Omega_{12}\hat{\rho}_{12}) - \gamma^r_{21}\hat{\rho}_{22} + \gamma^r_{32}\hat{\rho}_{33} + \hat{F}_{22} \\ \frac{\partial \hat{\rho}_{33}}{\partial t} &= 2\mathrm{Im}(\Omega_{03}\hat{\rho}_{03}) - \gamma^r_{30}\hat{\rho}_{33} - \gamma^r_{32}\hat{\rho}_{33} + \hat{F}_{33}\end{aligned} \tag{15}$$

The correlations $\langle \hat{F}_l \hat{F}_m\rangle$ of the stochastic forces are calculated from eq 14:

$$\begin{aligned}\langle \hat{F}_{12}\hat{F}^\dagger_{12}\rangle &= \left(\frac{d}{dt}\langle \hat{\rho}_{12}\hat{\rho}^\dagger_{12}\rangle\right)_{\text{NH}} - \langle -\Gamma_e \hat{\rho}_{12}\hat{\rho}^\dagger_{12}\rangle - \langle \hat{\rho}_{12}(-\Gamma_e \hat{\rho}^\dagger_{12})\rangle \\ &= \left\langle \frac{d}{dt}\rho_{11}\right\rangle_{\text{NH}} + 2\Gamma_e\rho_{11} = \gamma^r_{21}\rho_{22} - \gamma^r_{10}\rho_{11} + 2\Gamma_e\rho_{11} \\ \langle \hat{F}^\dagger_{12}\hat{F}_{12}\rangle &= \gamma^r_{32}\rho_{33} - \gamma^r_{21}\rho_{22} + 2\Gamma_e\rho_{22} \\ \langle \hat{F}_{03}\hat{F}^\dagger_{03}\rangle &= \gamma^r_{30}\rho_{33} + \gamma^r_{10}\rho_{11} + 2\Gamma_a\rho_{00} \\ \langle \hat{F}^\dagger_{03}\hat{F}_{03}\rangle &= -\gamma^r_{30}\rho_{33} - \gamma^r_{32}\rho_{33} + 2\Gamma_a\rho_{33} \\ \langle \hat{F}_{00}\hat{F}_{00}\rangle &= \left\langle \frac{d}{dt}\hat{\rho}_{00}\right\rangle_{\text{NH}} - 2\langle(\gamma^r_{30}\hat{\rho}_{33} + \gamma^r_{10}\hat{\rho}_{11})\hat{\rho}_{00}\rangle \\ &= \gamma^r_{30}\rho_{33} + \gamma^r_{10}\rho_{11} \\ \langle \hat{F}_{11}\hat{F}_{11}\rangle &= \gamma^r_{21}\rho_{22} + \gamma^r_{10}\rho_{11} \\ \langle \hat{F}_{22}\hat{F}_{22}\rangle &= \gamma^r_{32}\rho_{33} + \gamma^r_{21}\rho_{22} \\ \langle \hat{F}_{33}\hat{F}_{33}\rangle &= \gamma^r_{32}\rho_{33} + \gamma^r_{30}\rho_{33}\end{aligned} \tag{16}$$

In a typical four-level system $\gamma^r_{21} \approx \gamma^r_{30} \ll \gamma^r_{32} \approx \gamma^r_{10}$, and two of the relaxation noise terms can be neglected. Note, however, that for the validation performed below, the relaxation rates between the subsystems γ^r_{10} and γ^r_{32} are set to zero so that the terms proportional to γ^r_{21} and γ^r_{30} must be retained. Also, considering that in the nanoplasmonic metamaterial considered here there are a large numbers of photons and dipoles in the active medium that collectively participate in the coherent and fluctuation dynamics, we may apply the quantum-classical correspondence principle. In this spirit, the resulting semiclassical approach translates operator equations into c-number equations for a Hermitian density matrix. Therefore, we arrive at the following real-valued noise terms for the occupation densities that constitute the real-valued diagonal elements of the density matrix

$$\begin{aligned}F_{00} &= \xi_{10}\sqrt{\langle \hat{F}_{00}\hat{F}_{00}\rangle/N} = \xi_{10}\sqrt{\gamma^r_{10}\rho_{11}/N} \\ F_{11} &= -\xi_{10}\sqrt{\gamma^r_{10}\rho_{11}/N} \\ F_{22} &= \xi_{32}\sqrt{\gamma^r_{32}\rho_{33}/N} \\ F_{33} &= -\xi_{32}\sqrt{\gamma^r_{32}\rho_{33}/N}\end{aligned} \tag{17}$$

This formulation ensures that the trace of the density matrix $\hat{\rho}$ is conserved. For the polarization terms, we choose the normally ordered operator condition[18,30] to reduce the operator equations to c-number equations

$$\begin{aligned}F_{12} &= (\mathrm{Re}(\xi_{12}) + i\mathrm{Im}(\xi_{12}))\sqrt{\langle \hat{F}^\dagger_{12}\hat{F}_{12}\rangle/N} \\ &= (\mathrm{Re}(\xi_{12}) + i\mathrm{Im}(\xi_{12}))\sqrt{\frac{\gamma^r_{32}\rho_{33} + (2\Gamma_e - \gamma^r_{21})\rho_{22}}{2N}} \\ F_{03} &= (\mathrm{Re}(\xi_{03}) + i\mathrm{Im}(\xi_{03}))\sqrt{\langle \hat{F}^\dagger_{03}\hat{F}_{03}\rangle/N} \\ &= (\mathrm{Re}(\xi_{03}) + i\mathrm{Im}(\xi_{03}))\sqrt{\frac{(-\gamma^r_{32} + 2\Gamma_a - \gamma^r_{30})\rho_{33}}{2N}}\end{aligned} \tag{18}$$

Note that the noise terms for the density matrix elements scale inversely with the square root of the number of particles in the physical volume represented by the grid cell $N = \zeta N_{\text{cell}}$. This is due to the scaling properties of the standard deviation of a Gaussian distribution of independent random numbers. The noise levels used in the article are given by $\zeta = 10\,000$ for moderate noise (case 2) and $\zeta = 100$ for strong noise (case 3) and indicate the number of unit cells over which the noise is assumed to be coupled. For the mesoscopic system inside a grid cell, we assume isotropic coupling by introducing a polarization vector $\mathbf{P}_{e,a}$ driven by the electric field vector **E** and a scalar dipole strength for the emission e (2 ↔ 1) and absorption lines a (3 ↔ 0), resulting in independent Langevin noise terms for all three polarization directions.

Numerical Implementation. The numerical implementation of the four-level Maxwell-Bloch theory for amplification in active nanoplasmonic metamaterials[20] is described in detail by

Wuestner *et al.*[19] As we are here extending the approach by taking on board the interplay of noise with coherent amplification, a few comments are in place. To efficiently generate Gaussian random numbers with unit standard deviation, we use the Fortran implementation of the ziggurat algorithm[31] taken from http://www.netlib.org/random/ziggurat.f90. Also, it needs to be noted that, in the c-number approach, occupation densities may momentarily assume negative values. This does not constitute a problem as long as longer time averages stay within the range of physical values. Note, however, that in this case a practical computational issue may occur in the calculation of the noise terms because of the square root dependence, which we solve by using the absolute values. Moreover, as a consequence of the real-valued Maxwell-Bloch differential equations for the polarization being second-order in time, the polarization noise terms contain a time derivative. We calculate this time derivative by Euler forward integration

$$\left.\frac{\partial(\xi_1\sqrt{A})}{\partial t}\right|^{n+1} = (\xi_1^{n+1}\sqrt{A^{n+1}} - \xi_1^{n}\sqrt{A^{n}})/\Delta t \qquad (19)$$

where A denotes the term under the square root from eq 18. No systematic error accumulates, and no instabilities are expected using Euler forward integration for this time derivative since the individual terms are random. Finally, it should to be noted that in most cases the four-level model is used to approximate a molecular system with a multitude of individual energy levels being effectively combined into four levels by expressing the actual line width consisting of inhomogeneous and homogeneous broadening in terms of an effective homogeneous broadening process. However, only the broadening induced by dephasing contributes to the noise in the real molecular system. This is accounted for by replacing $\Gamma_{e,a}$ in eq 18 with the dephasing rate γ_d.

Transition from Superfluorescence to Amplified Spontaneous Emission. How can we test that amplification in our nanoplasmonic metamaterial is coherent and that the influence of noise is correctly grasped? Superfluorescence (SF) is a phenomenon of collective radiation from an ensemble of inverted atoms which is critically dependent on noise. Thereby the amplitude of the emission depends quadratically on the number of atoms, whereas the width of the peak depends inversely on the number of atoms. The pulse-width of the SF peak τ_r for a one-dimensional (1D) wire/pencil-shaped system (Fresnel number $F = A/\lambda L \approx 1$) is given by[32]

$$\tau_r = \frac{8\pi A T_1}{3\lambda^2 N_{ex}} \qquad (20)$$

with the relaxation time of the upper state population T_1, the area of the cylinder A, and the total number of inverted atoms N_{ex}. The time delay of the SF peak τ_d can be calculated as[32]

$$\tau_d = \frac{\tau_r}{4}(\ln(\sqrt{2\pi N_{ex}}))^2 \qquad (21)$$

Generally, the phenomenon of SF relies on the build up of coherence between the atoms in the emitting ensemble. So, if we observe a SF peak, we can expect coherence. However, small dephasing times (*i.e.*, fast dephasing rates) may lead to strong decoherence that can inhibit the build up of coherence. Due to the presence of amplification, this may lead, in turn, to amplified spontaneous emission (ASE), where it has been shown that the minimum dephasing time T_2 that determines the transition from SF to ASE is given by[32]

$$T_2 = \sqrt{\tau_r \tau_d} \qquad (22)$$

The build up of coherence is also inhibited if the number of atoms in the ensemble is too large leading to a maximum number N_c of atoms that will emit cooperatively

$$N_c = \frac{8\pi c T_1 A}{3\lambda^2 L} \qquad (23)$$

with L being the length of the wire-shaped system. If the number of atoms present is larger than N_c, SF still occurs but not all of the atoms will participate.

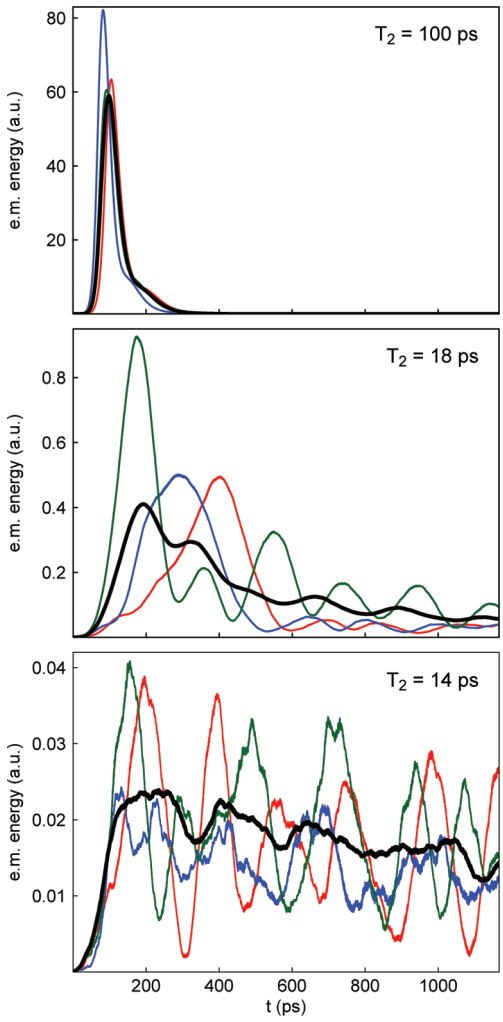

Figure 8. Transition from superfluorescence (SF) to amplified spontaneous emission (ASE) in a wire-shaped system as seen in the dynamics of the electromagnetic energy for T_2 = 100 ps (left), T_2 = 18 ps (middle), and T_2 = 14 ps (right). The thick black line shows the average over 10 randomly chosen realizations; the other (thinner) lines are randomly chosen results of individual runs.

To simulate SF,[21,33] one needs an ensemble of initially inverted two-level systems that are evenly distributed over a particular volume. For the purpose of this test of the real-valued polarization approach to the Maxwell-Bloch Langevin equations, we initially reduce the four-level system to a two-level system by setting the relaxation rates γ^r_{32} and γ^r_{10} to 0 and $\rho_{22} = 1$. The wire-shaped geometry results in an emission predominantly along the axis of the wire so that a one-dimensional representation is justified. In finite-difference time-domain simulation, a deep subwavelength resolution with a grid cell size that is substantially smaller than the emission wavelength of the atoms is needed. This grid cell represents the whole area of the transverse dimension (in our case a wire). Therefore, a grid cell of length dx represents the volume of Adx. This results in the volume ratio $\zeta = A/dx^2$, which has to be accounted for in the calculation of the noise terms. Furthermore, an initial tipping angle of the Bloch vector, consistent with the uncertainty relation, has to be assumed in order to start off SF. The magnitude of this tipping angle θ is inversely proportional to the square root of the number of atoms N represented by a grid cell $\theta = 2\xi_4/\sqrt{N}$, where ξ_4 is a Gaussian random variable with standard deviation of 1. The angle θ is calculated for each grid cell individually and an angle ϕ of the Bloch vector in the $x-y$

plane has to be drawn randomly at each position and translated into an initial phase of **P**.

In our test simulations, we use the (realistic) set of parameters: τ_d = 76 ps, τ_r = 2.7 ps, $(\tau_r\tau_d)^{1/2}$ = 14.4 ps, and $N_{ex} = 3 \times 10^8$, resulting in $N_c \approx 3.46 \times 10^8$. In this parameter regime, weak oscillatory SF (one peak with an oscillatory tail) should be observed for T_2 = 100 ps, and for T_2 = 14 ps, ASE is expected (see Figure 1 of Maki *et al.*[33] for the delineation of the regimes).

The results for simulations with T_2 = 100, 18, and 14 ps are shown in Figure 8. For a dephasing time of T_2 = 100 ps, we see weak oscillatory SF; for T_2 = 18 ps, we find SF with random modulations; and for T_2 = 14 ps, we find ASE, as expected.[33] These results confirm that the second-order in time formulation is a valid approach to a Langevin noise description in the four-level gain model.

Determination of Effective Electromagnetic Parameters. To determine experimentally accessible physical characteristics of (gain-enhanced) plasmonic nanostructures and metamaterials, we perform ultrafast time- and space-dependent pump−probe calculations, injecting short pulses with planar wavefronts for both the pump and probe fields onto the structure and determine *via* Fourier transformation spectrally resolved transmission and reflection spectra (local as well as spatially averaged). From the complex transmission $t(\omega)$ and reflection $r(\omega)$ coefficients, we can then calculate the spectral energy fluxes expressed in the transmission $T(\omega) = |t(\omega)|^2$, reflection $R(\omega) = |r(\omega)|^2$, and absorption $A(\omega) = 1 - T(\omega) - R(\omega)$. Adopting the methodology of Smith *et al.*,[25] one may extract effective electromagnetic parameters from the complex transmission, reflection, and absorption spectra. Retrieving these parameters allows one to examine the dispersion and signs of the real and imaginary parts of the homogenized refractive index, permittivity, and permeability.

The standard retrieval method is a general methodology for extracting the effective-medium parameters of a metamaterial,[34] making no assumption about the medium being either absorbing or amplifying. However, while this method is inherently applicable to active metamaterials, the sign of the retrieved index is usually chosen by requiring that $\mathrm{Im}(n_{eff}) \geq 0$. Clearly, in the presence of gain $\mathrm{Im}(n_{eff})$ can be negative, and this may complicate (but does not invalidate) the retrieval procedure. In that case, the causal and physically meaningful nature of the retrieved parameters has to be verified by checking whether Kramers−Kronig relations are obeyed[35]—a complementary methodology that has been applied successfully to loss-compensated metamaterials.[10−12,19] Yet, in the case of strong amplification (below the lasing threshold), as noted in the main text, it is not always possible to extract spectrally continuous effective-medium parameters.[12]

Conflict of Interest: The authors declare no competing financial interest.

Acknowledgment. Support by the Leverhulme Trust, the EPSRC and the Royal Academy of Engineering is gratefully acknowledged.

REFERENCES AND NOTES

1. Pendry, J. B. Negative Refraction Makes a Perfect Lens. *Phys. Rev. Lett.* **2000**, *85*, 3966–3969.
2. Fang, N.; Lee, H.; Sun, C.; Zhang, X. Sub-Diffraction-Limited Optical Imaging with a Silver Superlens. *Science* **2005**, *308*, 534–537.
3. Pendry, J. B. Optics: All Smoke and Metamaterials. *Nature* **2009**, *460*, 579–580.
4. Tsakmakidis, K. L.; Boardman, A. D.; Hess, O. `Trapped Rainbow' Storage of Light in Metamaterials. *Nature* **2007**, *450*, 397–401.
5. Gan, Q.; Fu, Z.; Ding, Y. J.; Bartoli, F. J. Ultrawide-Bandwidth Slow-Light System Based on THz Plasmonic Graded Metallic Grating Structures. *Phys. Rev. Lett.* **2008**, *100*, 256803.
6. Wegener, M.; García-Pomar, J. L.; Soukoulis, C. M.; Meinzer, N.; Ruther, M.; Linden, S. Toy Model for Plasmonic Metamaterial Resonances Coupled to Two-Level System Gain. *Opt. Express* **2008**, *16*, 19785–19798.
7. Plum, E.; Fedotov, V. A.; Kuo, P.; Tsai, D. P.; Zheludev, N. I. Towards the Lasing Spaser: Controlling Metamaterial Optical Response with Semiconductor Quantum Dots. *Opt. Express* **2009**, *17*, 8548–8551.
8. Fang, A.; Koschny, T.; Wegener, M.; Soukoulis, C. M. Self-Consistent Calculation of Metamaterials with Gain. *Phys. Rev. B* **2009**, *79*, 241104.
9. Sivan, Y.; Xiao, S.; Chettiar, U. K.; Kildishev, A. V.; Shalaev, V. M. Frequency-Domain Simulations of a Negative-Index Material with Embedded Gain. *Opt. Express* **2009**, *17*, 24060–24074.
10. Fang, A.; Koschny, T.; Soukoulis, C. M. Lasing in Metamaterial Nanostructures. *J. Opt.* **2010**, *12*, 024013.
11. Xiao, S.; Drachev, V. P.; Kildishev, A. V.; Ni, X.; Chettiar, U. K.; Yuan, H.-K.; Shalaev, V. M. Loss-Free and Active Optical Negative-Index Metamaterials. *Nature* **2010**, *466*, 735–738.
12. Wuestner, S.; Pusch, A.; Tsakmakidis, K. L.; Hamm, J. M.; Hess, O. Overcoming Losses with Gain in a Negative Refractive Index Metamaterial. *Phys. Rev. Lett.* **2010**, *105*, 127401.
13. Fang, A.; Koschny, T.; Soukoulis, C. M. Self-Consistent Calculations of Loss-Compensated Fishnet Metamaterials. *Phys. Rev. B* **2010**, *82*, 121102.
14. Meinzer, N.; Ruther, M.; Linden, S.; Soukoulis, C. M.; Khitrova, G.; Hendrickson, J.; Olitzky, J. D.; Gibbs, H. M.; Wegener, M. Arrays of Ag Split-Ring Resonators Coupled to InGaAs Single-Quantum-Well Gain. *Opt. Express* **2010**, *18*, 24140–24151.
15. Boardman, A. D.; Grimalsky, V. V.; Kivshar, Y. S.; Koshevaya, S. V.; Lapine, M.; Litchinitser, N. M.; Malnev, V. N.; Noginov, M.; Rapoport, Y. G.; Shalaev, V. M. Active and Tunable Metamaterials. *Laser Photonics Rev.* **2011**, *5*, 287–307.
16. Zuloaga, J.; Prodan, E.; Nordlander, P. Quantum Plasmonics: Optical Properties and Tunability of Metallic Nanorods. *ACS Nano* **2010**, *4*, 5269–5276.
17. Song, P.; Nordlander, P.; Gao, S. Quantum Mechanical Study of the Coupling of Plasmon Excitations to Atomic-Scale Electron Transport. *J. Chem. Phys.* **2011**, *134*, 074701.
18. Gardiner, C. W. *Quantum Noise*; Springer Verlag: Berlin, 1991.
19. Wuestner, S.; Pusch, A.; Tsakmakidis, K. L.; Hamm, J. M.; Hess, O. Gain and Plasmon Dynamics in Negative-Index Metamaterials. *Philos. Trans. R. Soc., A* **2011**, *369*, 3525–3550.
20. Hamm, J. M.; Wuestner, S.; Tsakmakidis, K. L.; Hess, O. Theory of Light Amplification in Active Fishnet Metamaterials. *Phys. Rev. Lett.* **2011**, *107*, 167405.
21. Andreasen, J.; Cao, H. Finite-Difference Time-Domain Formulation of Stochastic Noise in Macroscopic Atomic Systems. *J. Lightwave Technol.* **2009**, *27*, 4530.
22. Andreasen, J.; Cao, H. Spectral Behavior of Partially Pumped Weakly Scattering Random Lasers. *Opt. Express* **2011**, *19*, 3418–3433.
23. McMahon, J. A.; Wang, Y. M.; Sherry, L. J.; Van Duyne, R. P.; Marks, L. D.; Gray, S. K.; Schatz, G. C. Correlating the Structure, Optical Spectra, and Electrodynamics of Single Silver Nanocubes. *J. Phys. Chem. C* **2009**, *113*, 2731–2735.
24. Sperber, P.; Spangler, W.; Meier, B.; Penzkofer, A. Experimental and Theoretical Investigation of Tunable Picosecond Pulse Generation in Longitudinally Pumped Dye Laser Generators and Amplifiers. *Opt. Quantum Electron.* **1988**, *20*, 395–431.
25. Smith, D. R.; Schultz, S.; Markoš, P.; Soukoulis, C. M. Determination of Effective Permittivity and Permeability of Metamaterials from Reflection and Transmission Coefficients. *Phys. Rev. B* **2002**, *65*, 195104.
26. Mary, A.; Rodrigo, S. G.; Martn-Moreno, L.; Garca-Vidal, F. J. Holey Metal Films: From Extraordinary Transmission to Negative-Index Behavior. *Phys. Rev. B* **2009**, *80*, 165431.
27. Abraham, N. B.; Firth, W. J. Overview of Transverse Effects in Nonlinear-Optical Systems. *J. Opt. Soc. Am. B* **1990**, *7*, 951–962.
28. Drummond, P. D.; Raymer, M. G. Quantum Theory of Propagation of Nonclassical Radiation in a Near-Resonant Medium. *Phys. Rev. A* **1991**, *44*, 2072–2085.

29. Zardecki, A. Fluctuations of Optically Bistable Systems in the Bad-Cavity Limit. *Phys. Rev. A* **1981**, *23*, 1281–1289.
30. Ford, G. W.; Kac, M.; Mazur, P. Statistical Mechanics of Assemblies of Coupled Oscillators. *J. Math. Phys.* **1965**, *6*, 504–515.
31. Marsaglia, G.; Tsang, W. W. The Ziggurat Method for Generating Random Variables. *J. Stat. Soft.* **2000**, *5*, 1–7.
32. Malcuit, M. S.; Maki, J. J.; Simkin, D. J.; Boyd, R. W. Transition from Superfluorescence to Amplified Spontaneous Emission. *Phys. Rev. Lett.* **1987**, *59*, 1189–1192.
33. Maki, J. J.; Malcuit, M. S.; Raymer, M. G.; Boyd, R. W.; Drummond, P. D. Influence of Collisional Dephasing Processes on Superfluorescence. *Phys. Rev. A* **1989**, *40*, 5135–5142.
34. Cui, T. J.; Smith, D.; Liu, R. *Metamaterials: Theory, Design, and Applications*; Springer: New York, 2010.
35. Cook, J. J. H.; Tsakmakidis, K. L.; Hess, O. Ultralow-Loss Optical Diamagnetism in Silver Nanoforests. *J. Opt. A: Pure Appl. Opt.* **2009**, *11*, 114026.